



UNIVERSITY OF LEEDS

This is a repository copy of *Intrusion tip velocity controls the emplacement mechanism of sheet intrusions*.

White Rose Research Online URL for this paper:

<https://eprints.whiterose.ac.uk/205584/>

Version: Accepted Version

Article:

Kopping, J., Cruden, A.R., Thiele, S.T. et al. (2 more authors) (Accepted: 2023) Intrusion tip velocity controls the emplacement mechanism of sheet intrusions. *Geology*. ISSN 0091-7613 (In Press)

This item is protected by copyright. This is an author produced version of an article accepted for publication in *Geology*. Uploaded in accordance with the publisher's self-archiving policy.

Reuse

Items deposited in White Rose Research Online are protected by copyright, with all rights reserved unless indicated otherwise. They may be downloaded and/or printed for private study, or other acts as permitted by national copyright laws. The publisher or other rights holders may allow further reproduction and re-use of the full text version. This is indicated by the licence information on the White Rose Research Online record for the item.

Takedown

If you consider content in White Rose Research Online to be in breach of UK law, please notify us by emailing eprints@whiterose.ac.uk including the URL of the record and the reason for the withdrawal request.



eprints@whiterose.ac.uk
<https://eprints.whiterose.ac.uk/>

1 Intrusion tip velocity controls the emplacement mechanism of
2 sheet intrusions

3 **Jonas Köpping^{1,2}, Alexander R. Cruden², Samuel T. Thiele³, Craig Magee⁴, and Andrew**
4 **Bunger^{5,6}**

5 *¹ Department of Earth Sciences, ETH Zurich, 8092 Zurich, Switzerland*

6 *² School of Earth, Atmosphere and Environment, Monash University, Melbourne, 3800,*
7 *Australia*

8 *³ Helmholtz-Institute Dresden-Rossendorf, Institute Freiberg for Resource Technology, Freiberg,*
9 *Germany*

10 *⁴ School of Earth and Environment, University of Leeds, Leeds, LS2 9JT, UK*

11 *⁵ Department of Civil and Environmental Engineering, University of Pittsburgh, Pittsburgh, PA*
12 *15269, USA*

13 *⁶ Department of Chemical and Petroleum Engineering, University of Pittsburgh, Pittsburgh, PA*
14 *15269, USA*

15

16 **ABSTRACT**

17 Space for intruding magma is created by elastic, viscous, and/or plastic deformation of host rocks.
18 Such deformation impacts the geometries of igneous intrusions, particularly sills and dikes. For
19 example, tapered intrusion tips indicate linear-elastic fracturing during emplacement, whereas
20 fluidization of host rocks has been linked to development of elongate magma fingers with rounded
21 tips. Although host rock fluidization has only been observed at the lateral tips of magma fingers,
22 it is assumed to occur at their leading edges (frontal tips), and thereby control their propagation

23 and geometry. Here, we present macro- and microstructural evidence of fluidized sedimentary host
24 rock at the lateral tips of magma fingers emanating from the Shonkin Sag laccolith (Montana,
25 USA), and explore whether fluidization could have occurred at their frontal tips. Specifically, we
26 combine heat diffusion modelling and fracture tip velocity estimates to show that: (i) low intrusion
27 tip velocities ($\leq 10^{-5} \text{ m s}^{-1}$) allow pore fluids ahead of the intrusion to reach temperatures sufficient
28 to cause fluidization; but (ii) when tip velocities are high ($\sim 0.01\text{--}1 \text{ m s}^{-1}$), typical for many sheet
29 intrusions, fluidization ahead of propagating tips is inhibited. Our results suggest that intrusion tip
30 velocity (i.e., strain rate) is a first-order control on how rocks accommodate magma. Spatially and
31 temporarily varying velocities of lateral and frontal tips suggests deformation mechanisms at these
32 sites may be decoupled, meaning magma finger formation may not require host rock fluidization.
33 It is thus critical to consider strain rate and 3D intrusion geometry when inferring dominant magma
34 emplacement mechanisms.

35

36 INTRODUCTION

37 Igneous sheet intrusions (dikes and sills) often develop via the amalgamation of smaller building
38 blocks, here called “elements” (e.g., Pollard et al., 1975, 1982; Schofield et al., 2012; Wilson et
39 al., 2016; Köpping et al., 2022). Some elements have finger-like (or pipe-like) geometries, with
40 cross-sectional thickness-to-width ratios of $\sim 0.1\text{--}1$, which either coalesce into a continuous sheet
41 or propagate as isolated structures (Fig. 1A). Understanding the initiation and propagation of these
42 specific elements, often termed *magma fingers*, is important because they can control magma flow
43 localization (e.g., Köpping et al., 2023). Such localization of flow can impact magma storage and
44 eruption sites (e.g., Cashman and Sparks, 2013), and contribute to the accumulation of

45 orthomagmatic Ni-Cu-PGE sulphide deposits, which are often hosted in elongate, pipe-like
46 intrusions (e.g., Barnes et al., 2016).
47 Evidence for the disaggregation of host rocks by fluidization is often observed adjacent to the
48 *lateral* tips of finger-like elements (Fig. 1), which led to the interpretation that magma fingers form
49 by viscous fingering instabilities (Pollard et al., 1975; Schofield et al., 2010). However, as *frontal*
50 magma finger tips are rarely exposed in nature, we have to rely on modelling to test whether
51 fluidization can also occur at and drive the propagation of frontal magma finger tips. Here, we
52 combine structural field observations of lateral magma finger tips from the outer margin of the
53 Shonkin Sag laccolith (Montana, USA), with thermal modelling to evaluate whether the observed
54 deformation is analogous to that at unexposed frontal tips. Specifically, we assess whether host
55 rocks ahead of a propagating sheet intrusion can undergo significant fluidization to initiate the
56 formation of magma fingers (Schofield et al., 2010). Since dominant sheet intrusion emplacement
57 mechanisms are commonly inferred from host rock deformation observed near intrusion tips, our
58 work will further increase our knowledge on how magma migrates in the upper crust.

59

60 **SHEET INTRUSION ELEMENTS**

61 Field observations and 3D seismic reflection data indicate that element geometries range from
62 ribbon-like to pipe-like (Pollard et al., 1975, 1982; Galland et al., 2019; Stephens et al., 2021).
63 Ribbon-like elements are commonly vertically offset from each other, rotated about their long axis,
64 and associated with tensile-brittle magma emplacement (i.e., fracturing; e.g., Hutton, 2009;
65 Schofield et al., 2012; Magee et al., 2019; Stephens et al., 2021). In contrast, pipe-like elements
66 are often attributed to non-brittle magma emplacement mechanisms (e.g., Schofield et al., 2012).
67 Pollard et al. (1975) first coined the term *finger* or *magma finger* to describe pipe-like intrusions

68 that are exposed on the margin of the Shonkin Sag laccolith (Fig. 1), and suggested they formed
69 in response to the development of viscous instabilities at the magma–host rock contact.
70 Specifically, Pollard et al. (1975) related magma fingers to the phenomenon of viscous fingering,
71 which describes the unstable displacement of a high-viscosity fluid (i.e., fluidized host rock) by
72 one of a lower viscosity (i.e., magma; Saffman and Taylor, 1958). Such viscous fingering may
73 occur during: (i) intrusion-induced heating of local pore fluids, which increases their fluid pressure
74 beyond the brittle strength of the host rock (e.g., Kokelaar, 1982; Schofield et al., 2010); or (ii)
75 when secondary processes, such as overburden failure, cause a rapid pressure drop in the host rock
76 pore fluids (Schofield et al., 2010). These conditions can lead to boiling or flash boiling of the pore
77 fluids, respectively, driving their explosive expansion and disaggregating the sedimentary host
78 rock such that it can behave as a high viscosity fluid (e.g., Kokelaar, 1982; Schofield et al., 2010).
79 Evidence for such *thermal* and *triggered* host rock fluidization has been observed at the lateral
80 tips, and the top and bottom contacts of numerous sheet intrusions and magma fingers, but not
81 their frontal tips (e.g., Kokelaar, 1982; Schofield et al., 2010, 2012).

82

83 **GEOLOGICAL AND STRUCTURAL OBSERVATIONS**

84 The Shonkin Sag laccolith, located in the Highwood Mountains, MT, USA, formed at ca. 50 Ma
85 at a depth of ~1.4 km and consists of mafic shonkinite and syenite (Barksdale, 1937; Marvin et al.,
86 1980). The laccolith was emplaced into the tectonically undeformed Eagle Sandstone Formation,
87 a fine-grained Cretaceous sandstone with thin shale interbeds (Pollard et al., 1975). Five shonkinite
88 sills emerge from the SE margin of the laccolith and are well exposed along a ~1.8 km long, E-W
89 trending cliff face. These sills show evidence of coalesced and isolated m-scale magma fingers,

90 which propagated towards the SE along the sub-horizontal host rock bedding (Fig. 1B; Pollard et
91 al., 1975).

92 In cross sections oblique to the magma finger long axes, fingers at the SE margin of the Shonkin
93 Sag laccolith are 0.5–1.3 m thick and 1–13 m wide, with aspect ratios of 0.1–0.85 (Fig. 1B). In
94 addition to folding and shearing of host rock strata between magma fingers (Pollard et al., 1975),
95 evidence of host rock fluidization is commonly observed (Figs. 1B, 2). Specifically, juvenile clasts
96 of shonkinite mingle with sedimentary host rock to form *peperite* around lateral finger tips (Figs.
97 1B, 2). Irregularly-shaped fluidal clast morphologies indicate shearing between fluidized host rock
98 and intruding magma (Fig. 2; e.g., Skilling et al., 2002). These fluidal clasts are observed ≤ 1 m
99 from the exposed lateral finger tips (Fig. 2A). At the micro-scale, fragments of originally
100 continuous, flat-lying shale interlayers (< 1 cm thick) are dispersed and rotated within the peperite,
101 and they are crosscut locally by tensile fractures that do not extend into the sandstone matrix (Fig.
102 2B, i). Isolated quartz and feldspar grains float within a calcite and dolomite matrix, indicating
103 further evidence for host rock fluidization and mobilization (Fig. 2B, ii). Together, these
104 observations indicate that the sandstone was fluidized at the dm- to m-scale adjacent to the lateral
105 finger tips.

106

107 **ROLE OF INTRUSION TIP VELOCITY**

108 Field observations and numerical models of magma fingers are commonly limited to 2D lateral
109 tips (e.g., Pollard et al., 1975; Schofield et al., 2012; Souche et al., 2019; Stephens et al., 2021).

110 Despite this limitation, such data and models are used to infer finger formation and frontal
111 propagation mechanisms (e.g., Schofield et al., 2010, 2012; Spacapan et al., 2017). Here, we use
112 heat transfer modelling and fracture tip velocity estimates to constrain the conditions under which

113 host rock fluidization can occur. These calculations allow us to assess whether host rock
114 fluidization can initiate viscous fingering ahead of a propagating sheet intrusion.
115 Fluidization ahead of a propagating sill tip requires sufficient heat transfer to cause pore fluid
116 boiling ahead of the intrusion (e.g., Kokelaar, 1982; Schofield et al., 2010). Considering heat
117 transfer by thermal diffusion and, for simplicity, assuming negligible convective heat transfer, the
118 characteristic length (L_d) of heat diffusion ahead of an intrusion tip is:

$$119 \quad L_d = \sqrt{\kappa t} \quad (\text{Eq. 1}),$$

120 where κ = thermal diffusion ($\text{m}^2 \text{s}^{-1}$) and t = time (s) (Turcotte and Schubert, 2002). If L_d is greater
121 than the distance travelled by the intrusion tip ($L_{adv} = Ut$), moving at velocity U (m s^{-1}), heat from
122 the intruding magma diffuses into the host rocks at rates faster than tip propagation, and pore fluids
123 ahead of the propagating tip may reach temperatures sufficient for boiling to occur. The
124 temperature ahead of the intrusion, T , is then approximated by:

$$125 \quad T = T_\infty + (T_m - T_\infty)e^{-\frac{U}{\kappa}L} \quad (\text{Eq. 2}),$$

126 where T_∞ = background temperature (e.g., 52.5 °C at 1500 m depth), T_m = magma temperature
127 (1000–1200 °C for mafic magmas), and L = distance (m) ahead of the intrusion tip (Fig. 3A;
128 Supplemental Material 1; Turcotte and Schubert, 2002). For a reasonable value of κ for sandstone
129 ($1.3 \times 10^{-6} \text{ m}^2 \text{ s}^{-1}$; Geng et al., 2018), sill tip velocities between 10^{-5} and 10^{-6} m s^{-1} will heat pore
130 fluids to 300–350 °C within a distance of ~0.15 to 1.5 m ahead of the propagating intrusion,
131 respectively (Fig. 3B). These temperatures are sufficient to cause boiling at depths of 1–2 km
132 (Kokelaar, 1982), potentially fluidizing the sandstone and allowing viscous finger formation or
133 growth. Higher tip velocities ($\geq 10^{-4} \text{ m s}^{-1}$) only allow boiling ($T \geq 350$ °C) within ≤ 1.5 cm or flash
134 boiling ($T \geq 100$ °C) triggered by tensile host rock failure within ≤ 3.5 cm ahead of the intrusion
135 (Fig. 3B), which we consider insufficient to initiate meter-scale magma fingers. Our thermal

136 modelling approach assumes a constant heat source and represents the upper bound to heat transfer.
137 The results indicate that thermal and triggered host rock fluidization are only likely to occur when
138 intrusion tip velocities are low ($\leq 10^{-5}$ m s⁻¹), which contrasts with high tip velocities of up to 1 m
139 s⁻¹ assumed in previous studies (Schofield et al., 2010).
140 Because our calculations suggest fluidization requires low intrusion tip velocities, it is useful to
141 mechanistically bound the tip velocities based on measured apertures of fluid-driven fractures,
142 assuming linear-elastic fracturing as initial emplacement mechanism (e.g., Gudmundsson, 2011).
143 For the case where the tip advance is driven by a viscous fluid and the host rock is elastic, the tip
144 velocity (V) of a hydro-fracture propagating in a regime where the dynamics are determined by
145 the viscosity of the fracture fluid is approximated by:

$$146 \quad V \sim \frac{E' w^3}{216 \sqrt{3} \mu s^2} \quad (\text{Eq. 3}),$$

147 where E' = plane strain modulus, μ = fluid viscosity, w = fracture opening, and s = distance
148 between w -measurement and the fracture tip (Fig. 3C; Desroches et al., 1994; Detournay, 2016;
149 Xing et al., 2017). To approximate intrusion tip velocities, we use field constraints for w and s
150 from sills and dikes with sharp tip geometries, which suggest propagation via linear-elastic
151 fracturing (Supplemental Material 1, 2; Galland et al., 2018; Poppe et al., 2020; Schmiedel et al.,
152 2021; Walker et al., 2021). Using this approach, low tip velocities ($< 10^{-5}$ m s⁻¹) required to cause
153 pore fluid boiling and host rock fluidization can be achieved by high-viscosity ($\mu \geq 10^8$ Pa s) felsic
154 or crystal-rich magmas, but not by low-viscosity mafic magmas such as shonkinite (Fig. 3D;
155 Murase and McBirney, 1973).

156

157 **DISCUSSION AND CONCLUSIONS**

158 Frequent observations of fluidized host rock in the vicinity of magma fingers may support an
159 interpretation linking fluidization and magma finger formation via viscous instabilities (Pollard et
160 al. 1975; Schofield et al., 2010, 2012). However, our modelling suggests that host rocks will not
161 undergo fluidization when the magma propagation velocity is representative of laterally
162 propagating sheet intrusions ($\sim 0.01\text{--}1\text{ m s}^{-1}$; e.g., Ágústsdóttir et al., 2016). The initiation of
163 magma fingers may therefore not be due to viscous fingering caused by host rock fluidization.
164 Instead, we hypothesize that the fluidized host rocks observed adjacent to magma fingers are linked
165 to the different propagation velocities between frontal versus lateral tips (Fig. 4). Variable stress
166 accumulation at intrusion tips (Walker et al., 2021), local changes in emplacement conditions such
167 as natural variations in pore fluid content and host rock matrix strength (Stephens et al., 2021), or
168 overlapping temperature halos of adjacent magma fingers may explain the irregular occurrence of
169 fluidization in the vicinity of magma fingers (Fig. 1B) and may affect host rock deformation.
170 Critically, the elongate 3D geometry of magma fingers implies higher velocity (i.e., higher strain
171 rate) at the frontal tips, causing lengthening, and lower velocity (i.e., lower strain rate) at lateral
172 tips, causing finger widening and coalescence (Fig. 4A), which has been confirmed by 3D
173 laboratory experiments (Arachchige et al., 2022). Lateral finger tips are therefore unlikely to
174 propagate by the same mechanism as frontal tips. Linking magma fingers to potential high strain
175 rate regimes will contribute to unravelling their initiation and propagation mechanisms, and as
176 such to better understanding the formation of orthomagmatic Ni-Cu-PGE deposits, which are often
177 hosted in mafic and ultramafic, elongate or pipe-like intrusions in which magma flow can
178 channelize (Barnes et al., 2016).

179 Overall, we suggest that low velocity propagation, associated with low strain rates, and a
180 continuous heat supply, combined with local stress accumulation at lateral finger tips make these

181 favorable sites for host rock fluidization (Fig. 4B). Deformation features observed at lateral tips
182 therefore reflect intrusion widening and vertical inflation rather than finger formation or
183 lengthening, from which they are decoupled spatially and temporally due to the differences in
184 strain rates and thermal regimes. Tip velocity and strain rate are thus key, but largely ignored,
185 parameters that control how host rocks accommodate magma emplacement. As the tip velocity of
186 elements (e.g., fingers), or entire sheet intrusions, varies spatially along their edges (e.g., frontal
187 tip velocities of bladed dikes or elongate sills are faster than their lateral tips; Townsend et al.,
188 2017; Davis et al., 2021), interpreting magma emplacement mechanisms based on 2D outcrop
189 observations may not fully capture all the processes accommodating emplacement. Furthermore,
190 our findings suggest magma emplacement mechanisms could be temporally variable throughout
191 their lifespan, requiring caution when inferring dominant magma emplacement mechanisms in the
192 upper crust from final intrusion forms and associated host rock deformation.

193

194 **ACKNOWLEDGEMENTS**

195 We are grateful to Mr. and Mrs. Ebeling for permitting access to the cliff faces of the Shonkin Sag
196 laccolith. We thank Anja Slim for her support with heat diffusion modelling and Richard Walker
197 for providing photographs of sill tips. We gratefully acknowledge helpful reviews from Penelope
198 Wilson, Steffi Burchardt, and an anonymous reviewer, and we thank Robert Holdsworth for his
199 editorial handling of the manuscript. JK was supported by a Monash Graduate Scholarship and a
200 Graduate Research Completion Award. ARC and CM were supported by Australian Research
201 Council Discovery Grant DP190102422.

202 **REFERENCES**

- 203 Ágústsdóttir, T., Woods, J., Greenfield, T., Green, R.G., White, R.S., Winder, T., Brandsdóttir,
204 B., Steinthórsson, S., and Soosalu, H., 2016, Strike-slip faulting during the 2014
205 Bárðarbunga-Holuhraun dike intrusion, central Iceland: *Geophysical Research Letters*, v.
206 43, p. 1495–1503, doi:10.1002/2015GL067423.
- 207 Arachchige, U.N., Cruden, A.R., Weinberg, R., Slim, A., and Köpping, J., 2022, Saucers,
208 Fingers, and Lobes: New Insights on Sill Emplacement From Scaled Laboratory
209 Experiments: *Journal of Geophysical Research: Solid Earth*, v. 127, p. e2022JB024421,
210 doi:10.1029/2022JB024421.
- 211 Barksdale, J.D., 1937, The Shonkin Sag laccolith: *American Journal of Science*, v. 33, p. 321–
212 359.
- 213 Barnes, S.J., Cruden, A.R., Arndt, N., and Saumur, B.M., 2016, The mineral system approach
214 applied to magmatic Ni–Cu–PGE sulphide deposits: *Ore Geology Reviews*, v. 76, p.
215 296–316, doi:10.1016/j.oregeorev.2015.06.012.
- 216 Cashman, K.V., and Sparks, R.S.J., 2013, How volcanoes work: A 25 year perspective: *Bulletin*
217 of the Geological Society of America, v. 125, p. 664–690, doi:10.1130/B30720.1.
- 218 Davis, T., Bagnardi, M., Lundgren, P., and Rivalta, E., 2021, Extreme Curvature of Shallow
219 Magma Pathways Controlled by Competing Stresses: Insights From the 2018 Sierra
220 Negra Eruption: *Geophysical Research Letters*, v. 48, p. e2021GL093038,
221 doi:10.1029/2021GL093038.
- 222 Desroches, J., Detournay, E., Lenoach, B., Papanastasiou, P., Pearson, J.P.A., Thiercelin, M., and
223 Cheng, A., 1994, The crack tip region in hydraulic fracturing: *Proceedings of the Royal*
224 Society of London. Series A: Mathematical and Physical Sciences, v. 447, p. 39–48,
225 doi:10.1098/rspa.1994.0127.
- 226 Detournay, E., 2016, Mechanics of Hydraulic Fractures: *Annual Review of Fluid Mechanics*, v.
227 48, p. 311–339, doi:10.1146/annurev-fluid-010814-014736.
- 228 Galland, O. et al., 2018, Storage and Transport of Magma in the Layered Crust—Formation of
229 Sills and Related Flat-Lying Intrusions, *in* *Volcanic and Igneous Plumbing Systems*,
230 Elsevier, p. 113–138, doi:10.1016/B978-0-12-809749-6.00005-4.
- 231 Galland, O., Spacapan, J.B., Rabbel, O., Mair, K., Soto, F.G., Eiken, T., Schiuma, M., and
232 Leanza, H.A., 2019, Structure, emplacement mechanism and magma-flow significance of
233 igneous fingers – Implications for sill emplacement in sedimentary basins: *Journal of*
234 Structural Geology, v. 124, p. 120–135, doi:10.1016/j.jsg.2019.04.013.
- 235 Geng, J., Sun, Q., Zhang, Y., Cao, L., Lü, C., and Zhang, Y., 2018, Temperature dependence of
236 the thermal diffusivity of sandstone: *Journal of Petroleum Science and Engineering*, v.
237 164, p. 110–116, doi:10.1016/j.petrol.2018.01.047.

- 238 Gudmundsson, A., 2011, *Rock Fractures in Geological Processes*: Cambridge, New York,
239 Cambridge University Press, 1–569 p.
- 240 Hutton, D.H.W., 2009, Insights into magmatism in volcanic margins: bridge structures and a new
241 mechanism of basic sill emplacement - Theron Mountains, Antarctica: *Petroleum*
242 *Geoscience*, v. 15, p. 269–278, doi:10.1144/1354-079309-841.
- 243 Kokelaar, B.P., 1982, Fluidization of wet sediments during the emplacement and cooling of
244 various igneous bodies: *Journal of the Geological Society*, v. 139, p. 21–33,
245 doi:10.1144/gsjgs.139.1.0021.
- 246 Köpping, J., Cruden, A.R., Magee, C., McCarthy, W., Geissman, J., and Holm, D., 2023,
247 Magnetic fabrics reveal three-dimensional flow processes within elongate magma fingers
248 at the margin of the Shonkin Sag laccolith (MT, USA): *Journal of Structural Geology*, v.
249 169, p. 104829, doi:10.1016/j.jsg.2023.104829.
- 250 Köpping, J., Magee, C., Cruden, A.R., Jackson, C.A.-L., and Norcliffe, J.R., 2022, The building
251 blocks of igneous sheet intrusions: Insights from 3-D seismic reflection data: *Geosphere*,
252 doi:10.1130/GES02390.1.
- 253 Magee, C., Muirhead, J., Schofield, N., Walker, R.J., Galland, O., Holford, S., Spacapan, J.,
254 Jackson, C.A.L., and McCarthy, W., 2019, Structural signatures of igneous sheet
255 intrusion propagation: *Journal of Structural Geology*, v. 125, p. 148–154,
256 doi:10.1016/j.jsg.2018.07.010.
- 257 Marvin, R.F., Hearn Jr., B.O., Mehnert, H.H., Naesser, C.W., Zartman, R.E., and Lindsley, D.A.,
258 1980, Late Cretaceous-Paleocene igneous activity in north-central Montana:
259 *Isochron/West*, v. 29, p. 5–25.
- 260 Murase, T., and McBirney, A.R., 1973, Properties of Some Common Igneous Rocks and Their
261 Melts at High Temperatures: *Geological Society of America Bulletin*, v. 84, p. 3563,
262 doi:10.1130/0016-7606(1973)84<3563:POSCIR>2.0.CO;2.
- 263 Pollard, D.D., Muller, O.H., and Dockstader, D.R., 1975, The form and growth of fingered sheet
264 intrusions: *Geological Society of America Bulletin*, v. 86, p. 351–363, doi:10.1130/0016-
265 7606(1975)86<351:TFAGOF>2.0.CO;2.
- 266 Pollard, D.D., Segall, P., and Delaney, P.T., 1982, Formation and interpretation of dilatant
267 echelon cracks.: *Geological Society of America Bulletin*, v. 93, p. 1291–1303,
268 doi:10.1130/0016-7606(1982)93<1291:FAIODE>2.0.CO;2.
- 269 Poppe, S., Galland, O., de Winter, N.J., Goderis, S., Claeys, P., Debaille, V., Boulvais, P., and
270 Kervyn, M., 2020, Structural and Geochemical Interactions Between Magma and
271 Sedimentary Host Rock: The Hovedøya Case, Oslo Rift, Norway: *Geochemistry*,
272 *Geophysics, Geosystems*, v. 21, p. 1–22, doi:10.1029/2019GC008685.

- 273 Saffman, P.G., and Taylor, G.I., 1958, The penetration of a fluid into a porous medium or Hele-
274 Shaw cell containing a more viscous liquid: Dynamics of Curved Fronts, v. 245, p. 312–
275 329, doi:10.1016/B978-0-08-092523-3.50017-4.
- 276 Schmiedel, T., Burchardt, S., Mattsson, T., Guldstrand, F., Galland, O., Palma, J., and Skogby,
277 H., 2021, Emplacement and Segment Geometry of Large, High-Viscosity Magmatic
278 Sheets: *Minerals*, v. 11, p. 1113, doi:10.3390/min11101113.
- 279 Schofield, N.J., Brown, D.J., Magee, C., and Stevenson, C.T., 2012, Sill morphology and
280 comparison of brittle and non-brittle emplacement mechanisms: *Journal of the Geological*
281 *Society*, v. 169, p. 127–141, doi:10.1144/0016-76492011-078.
- 282 Schofield, N.J., Stevenson, C., and Reston, T., 2010, Magma fingers and host rock fluidization in
283 the emplacement of sills: *Geology*, v. 38, p. 63–66, doi:10.1130/G30142.1.
- 284 Skilling, I.P., White, J.D.L., and McPhie, J., 2002, Peperite: A review of magma-sediment
285 mingling: *Journal of Volcanology and Geothermal Research*, v. 114, p. 1–17,
286 doi:10.1016/S0377-0273(01)00278-5.
- 287 Souche, A., Galland, O., Haug, Ø.T., and Dabrowski, M., 2019, Impact of host rock
288 heterogeneity on failure around pressurized conduits: Implications for finger-shaped
289 magmatic intrusions: *Tectonophysics*, v. 765, p. 52–63, doi:10.1016/j.tecto.2019.05.016.
- 290 Spacapan, J.B., Galland, O., Leanza, H.A., and Planke, S., 2017, Igneous sill and finger
291 emplacement mechanism in shale-dominated formations: a field study at Cuesta del
292 Chihuido, Neuquén Basin, Argentina: *Journal of the Geological Society*, v. 174, p. 422–
293 433, doi:10.1144/jgs2016-056.
- 294 Stephens, T., Walker, R., Healy, D., and Bubeck, A., 2021, Segment tip geometry of sheet
295 intrusions, II: Field observations of tip geometries and a model for evolving emplacement
296 mechanisms: *Volcanica*, v. 4, p. 203–225, doi:10.30909/vol.04.02.203225.
- 297 Townsend, M.R., Pollard, D.D., and Smith, R.P., 2017, Mechanical models for dikes: A third
298 school of thought: *Tectonophysics*, v. 703–704, p. 98–118,
299 doi:10.1016/j.tecto.2017.03.008.
- 300 Turcotte, D.L., and Schubert, G., 2002, *Geodynamics*: Cambridge University Press, v. 2.
- 301 Walker, R., Stephens, T., Greenfield, C., Gill, S., Healy, D., and Poppe, S., 2021, Segment tip
302 geometry of sheet intrusions, I: Theory and numerical models for the role of tip shape in
303 controlling propagation pathways: *Volcanica*, v. 4, p. 189–201,
304 doi:10.30909/vol.04.02.189201.
- 305 Wilson, P.I.R., McCaffrey, K.J.W., Wilson, R.W., Jarvis, I., and Holdsworth, R.E., 2016,
306 Deformation structures associated with the Trachyte Mesa intrusion, Henry Mountains,
307 Utah: Implications for sill and laccolith emplacement mechanisms: *Journal of Structural*
308 *Geology*, v. 87, p. 30–46, doi:10.1016/j.jsg.2016.04.001.

309 Xing, P., Yoshioka, K., Adachi, J., El-Fayoumi, A., and Bungler, A.P., 2017, Laboratory
310 measurement of tip and global behavior for zero-toughness hydraulic fractures with
311 circular and blade-shaped (PKN) geometry: *Journal of the Mechanics and Physics of*
312 *Solids*, v. 104, p. 172–186, doi:10.1016/j.jmps.2017.04.013.

313

314 **FIGURE CAPTIONS**

315 Figure 1. (A) Schematic 3D diagram shows elongate magma fingers emerging from a continuous
316 sheet. Schematic 2D cross-sections show coalesced and separate magma fingers. (B) Photograph
317 shows cross-sectional outcrop of individual magma fingers at the outer margin of the Shonkin Sag
318 laccolith. Magma emplacement-related host rock deformation at lateral tips is indicated in (A) and
319 (B).

320

321 Figure 2. (A) Photograph and sketch interpretation of an oblique cross-section through a magma
322 finger, revealing peperite adjacent to a lateral tip. Inset shows a fluidal shonkinite clast
323 morphology. (B) Thin sections of a peperite sample scanned under crossed polarized light showing
324 juvenile shonkinite clasts and shale fragments mingled with mobilized host rock. High-angle
325 fractures in shale layers do not extend into the sandstone (i) and quartz and feldspar grains floating
326 in a matrix of calcite and dolomite (ii) highlight that the sandstone was fluidized. Note that thin
327 sections show representative examples of fluidized sandstone adjacent to the Shonkin Sag magma
328 fingers.

329

330 Figure 3. (A, B) Temperature (T) ahead of a propagating intrusion tip, at a specific length (L)
331 calculated for a range of sill tip velocities (U) using Eq. 2. (C, D) Fracture tip velocities (V) for a
332 range of magma viscosities (μ) estimated using Eq. 3.

333

334 Figure 4. (A) Schematic map-view time-series shows the propagation and formation of elongate
335 sheet intrusions (t_0) and magma fingers (t_1, t_2). Lateral and frontal intrusions tips and temperature
336 contours are indicated. (B) Schematic block diagram highlights the difference in temperature

337 around frontal and lateral intrusion tips with high and low tip velocities, respectively. Regions
338 where host rock fluidization is likely to occur are indicated.

Width: 118 mm
Height: 135 mm

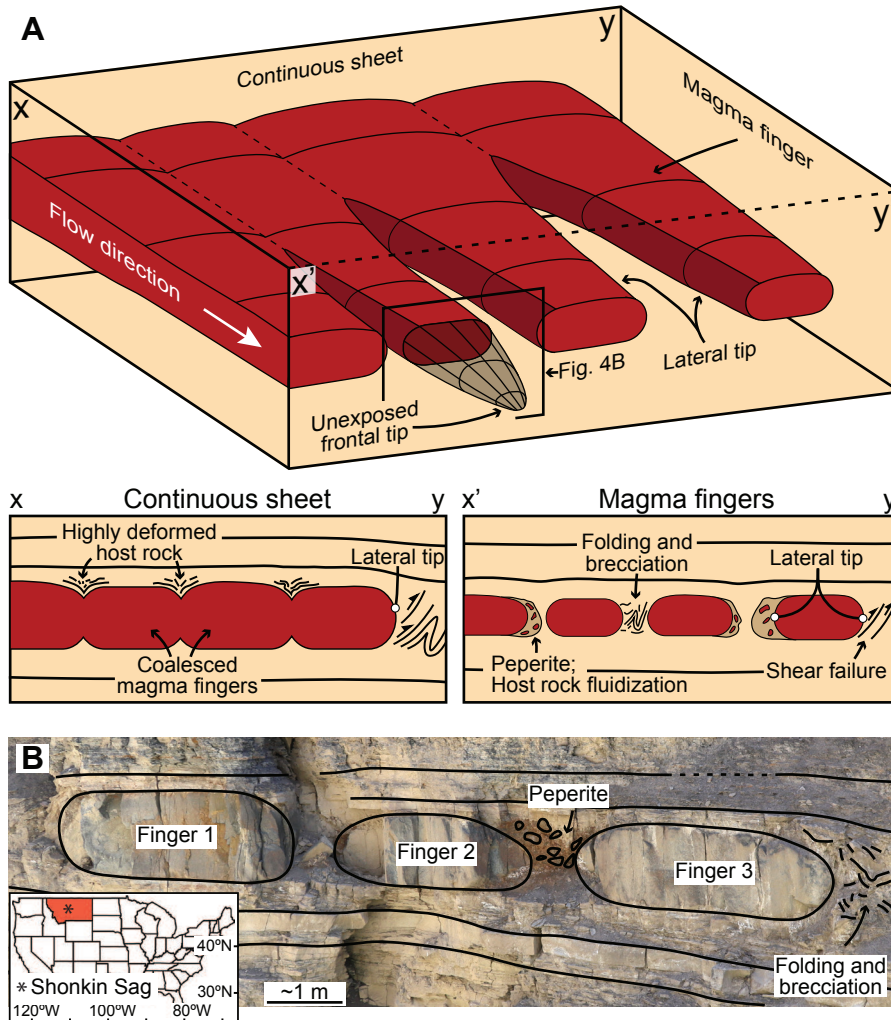


Figure 1. (A) Schematic 3D diagram shows elongate magma fingers emerging from a continuous sheet. Schematic 2D cross-sections show coalesced and separate magma fingers. (B) Photograph shows cross-sectional outcrop of individual magma fingers at the outer margin of the Shonkin Sag laccolith. Magma emplacement-related host rock deformation at lateral tips is indicated in (A) and (B).

Width: 118 mm
Height: 130 mm

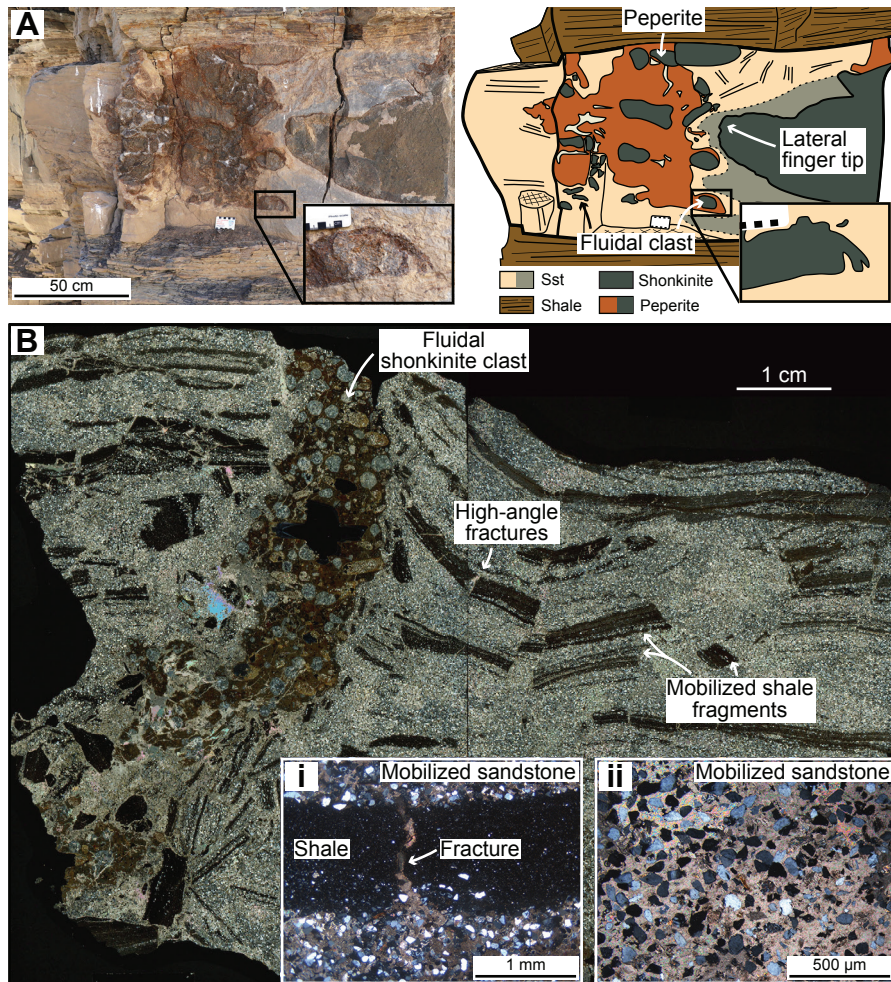


Figure 2. (A) Photograph and sketch interpretation of an oblique cross-section through a magma finger, revealing peperite adjacent to a lateral tip. Inset shows a fluidal shonkinite clast morphology. (B) Thin sections of a peperite sample scanned under crossed polarized light showing juvenile shonkinite clasts and shale fragments mingled with mobilized host rock. High-angle fractures in shale layers do not extend into the sandstone (i) and quartz and feldspar grains floating in a matrix of calcite and dolomite (ii) highlight that the sandstone was fluidized. Note that thin sections show representative examples of fluidized sandstone adjacent to the Shonkin Sag magma fingers.

Width: 177 mm
Height: 94 mm

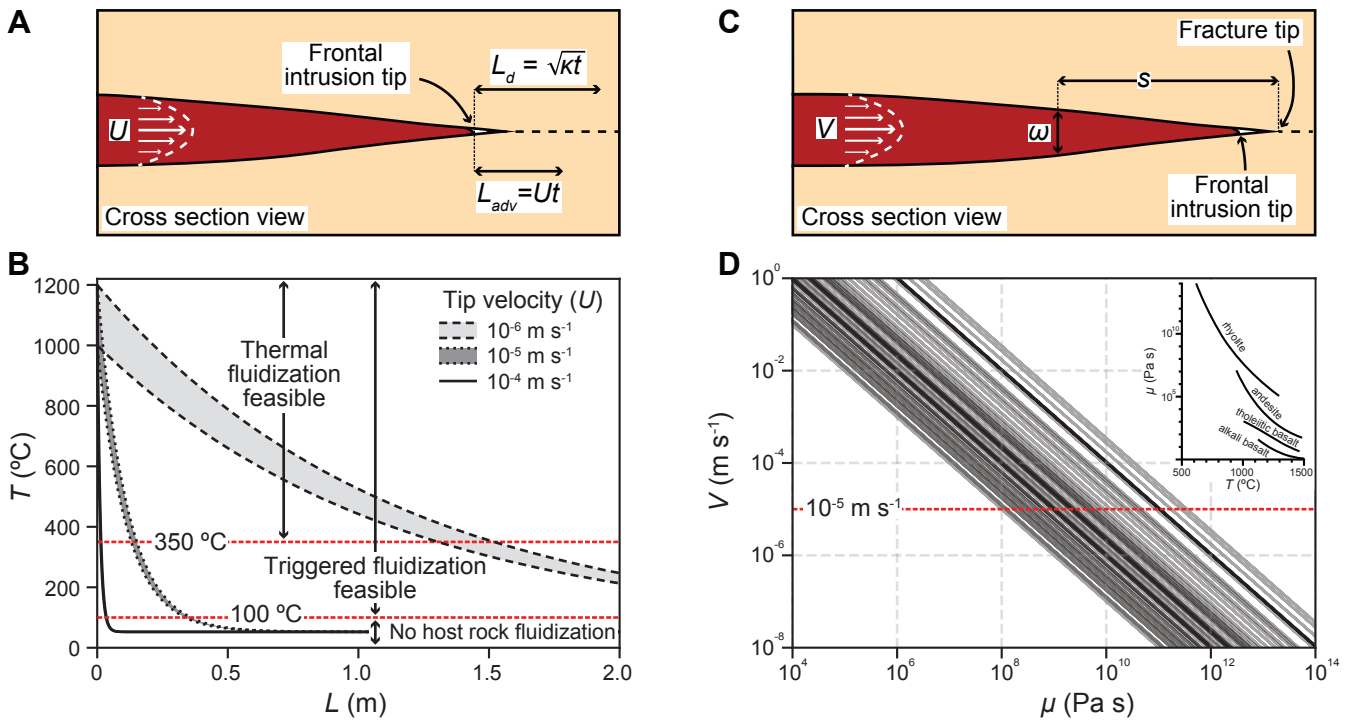


Figure 3. (A, B) Temperature (T) ahead of a propagating intrusion tip, at a specific length (L) calculated for a range of sill tip velocities (U) using Eq. 2. (C, D) Fracture tip velocities (V) for a range of magma viscosities (μ) estimated using Eq. 3.

Width: 118 mm
Height: 112 mm

A Map-view time-series

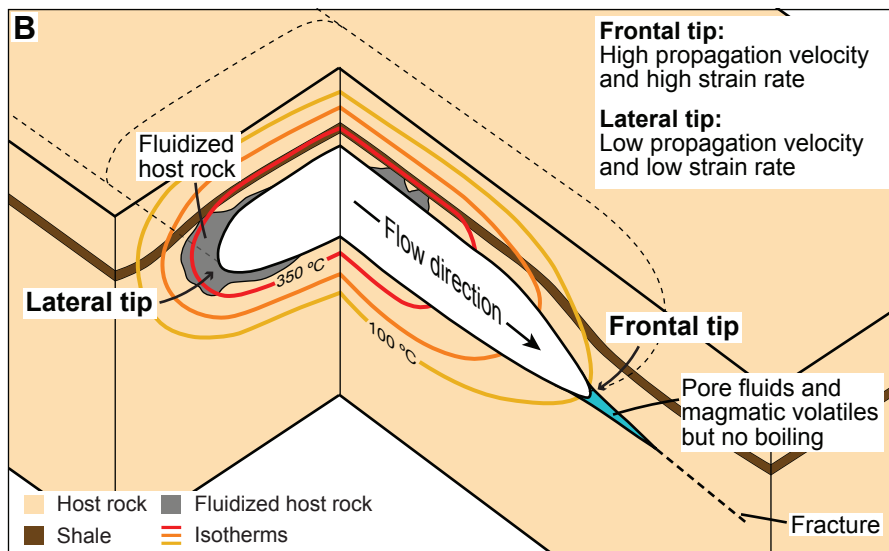
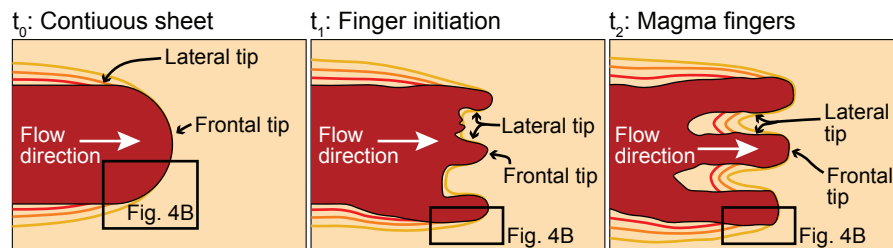


Figure 4. (A) Schematic map-view time-series shows the propagation and formation of elongate sheet intrusions (t_0) and magma fingers (t_1, t_2). Lateral and frontal intrusion tips and temperature contours are indicated. (B) Schematic block diagram highlights the difference in temperature around frontal and lateral intrusion tips with high and low tip velocities, respectively. Regions where host rock fluidization is likely to occur are indicated.